Acta Crystallographica Section D
Biological Crystallography
ISSN 0907-4449

Getting the best out of long-wavelength X-rays: *de novo* chlorine/sulfur SAD phasing of a structural protein from ATV

Adeline Goulet,[a] Gisle Vestergaard,[b] Catarina Felisberto-Rodrigues,[a] Valérie Campanacci,[a] Roger A. Garrett,[b] Christian Cambillau[a] and Miguel Ortiz-Lombardía[a]*

[a]Architecture et Fonction des Macromolécules Biologiques UMR 6098, CNRS, Universités d'Aix-Marseille I et II, Case 932, 163 Avenue de Luminy, 13288 Marseille CEDEX 9, France, and [b]Danish Archaea Centre, Department of Biology, Copenhagen University, Ole Maales Vej 5, 2200 Copenhagen, Denmark

Correspondence e-mail: miguel@afmb.univ-mrs.fr

Received 31 August 2009
Accepted 1 December 2009

PDB Reference: Structural protein from the *Acidianus* two-tailed virus, 3faj.

The structure of a 14 kDa structural protein from *Acidianus* two-tailed virus (ATV) was solved by single-wavelength anomalous diffraction (SAD) phasing using X-ray data collected at 2.0 Å wavelength. Although the anomalous signal from methionine sulfurs was expected to suffice to solve the structure, one chloride ion turned out to be essential to achieve phasing. The minimal data requirements and the relative contributions of the Cl and S atoms to phasing are discussed. This work supports the feasibility of a systematic approach for the solution of protein crystal structures by SAD based on intrinsic protein light atoms along with associated chloride ions from the solvent. In such cases, data collection at long wavelengths may be a time-efficient alternative to selenomethionine substitution and heavy-atom derivatization.

1. Introduction

The power of single-wavelength anomalous diffraction (SAD) was illustrated almost 30 years ago by Hendrickson and Teeter, who used the anomalous signal from six S atoms to solve the structure of the 4.8 kDa protein crambin (Hendrickson & Teeter, 1981). In recent years, SAD has become the method of choice for *de novo* phasing (Rice *et al.*, 2000; Dodson, 2003) after gaining popularity as an easier and more time-efficient alternative to multi-wavelength anomalous diffraction (MAD) experiments. The SAD method, which requires a single set of data and hence minimizes the effects of radiation damage, benefits from methodological advances in X-ray crystallography such as (i) the availability of tunable synchrotron beamlines for data collection, (ii) cryogenic techniques, (iii) accurate detectors with short readout time and (iv) improved software for data processing, phasing and density modification. However, the anomalous difference ($\Delta F^{\pm}$) is a weak signal. Based on simulated error-free structure factors of a 12 kDa protein, Wang concluded that an anomalous signal ($\langle\Delta F^{\pm}\rangle/\langle F\rangle$) as low as 0.6%, if accurately measured, could be sufficient for successful SAD phasing (Wang, 1985). More recently, Zwart has shown that for data including errors a plot of the measurability of Bijvoet differences *versus* resolution can be used to judge the quality and amount of the anomalous signal (Zwart, 2005).

The most frequently used anomalous scatterers are either inherently contained in metalloproteins (*e.g.* Zn, Fe or Cu) or are introduced by heavy-atom derivatization (*e.g.* Hg, Pt, lanthanides and actinides) or by recombinant DNA methods, as in selenomethionine substitution. Although efficient strategies and protocols have been described for selenomethionine substitution (Doublié, 1997) and heavy-atom derivatization (Garman & Murray, 2003), these steps stand as bottlenecks in the structure-solution process. Thus, a trend is developing towards the solution of the phase problem from 'native' crystals of macromolecules using softer X-rays and intrinsic lighter atoms such as sulfur for proteins, phosphorus for nucleic acids (Dauter & Adamiak, 2001) and cofactor metals such as manganese (Ramagopal *et al.*, 2003*a*; Salgado *et al.*, 2005). Besides, light atoms such as chlorine and calcium, which are widely used in crystallization,

Table 1
Data-collection and processing statistics.

Values in parentheses are for the highest resolution shell, namely 1.80–1.70 Å for the native data set and 2.85–2.70 Å for the SAD data sets.

	Native	sad1	sad2	sad3	sad4	sad5	sad6	sad7	sad8
No. of images	150	440	440	440	440	431	439	419	440
κ (°)	0	0	30	−30	30	−15	15	−10	10
φ (°)	0	0	0	0	180	0	0	0	0
Unique reflections	13953 (1993)	3471 (479)	3477 (474)	3487 (487)	3480 (481)	3474 (480)	3484 (488)	3491 (486)	3492 (486)
Completeness (%)	99.3 (99.3)	98.9 (93.0)	98.8 (91.9)	99.1 (94.4)	98.9 (92.5)	98.6 (92.3)	98.9 (93.5)	98.8 (92.6)	98.8 (92.4)
Multiplicity†	4.6 (4.6)	6.0 (3.1)	6.0 (3.1)	6.0 (3.0)	6.0 (3.1)	5.8 (3.0)	5.9 (3.0)	5.6 (3.0)	5.9 (3.1)
$\langle I/\sigma(I)\rangle$	15.5 (3.1)	41.7 (15.0)	30.0 (7.4)	47.3 (19.6)	40.8 (14.9)	52.3 (23.2)	41.8 (14.2)	37.1 (10.5)	20.3 (4.5)
$R_{\rm meas}$‡ (%)	7.2 (51.5)	4.7 (9.1)	7.0 (21.9)	4.4 (7.3)	5.1 (11.4)	3.9 (5.8)	4.9 (10.0)	5.6 (15.3)	8.5 (43.3)
$R_{\rm p.i.m.}$§ (%)	3.4 (26.8)	1.3 (3.7)	2.0 (8.7)	1.2 (3.1)	1.5 (4.6)	1.1 (2.4)	1.4 (4.2)	1.7 (6.3)	2.9 (15.9)
$R_{\rm anom}$¶	—	4.0 (9.5)	5.4 (19.6)	3.8 (8.0)	4.1 (9.7)	3.4 (6.8)	3.8 (10.5)	4.6 (13.8)	6.9 (33.1)
Anomalous signal to noise††	—	1.2 (0.8)	1.0 (0.7)	1.3 (0.8)	1.2 (0.8)	1.4 (1.0)	1.1 (0.7)	1.0 (0.7)	0.9 (0.8)

	sad1–2	sad1–3	sad1–4	sad1–5	sad1–6	sad1–7	sad1–8
Multiplicity†	11.8 (5.5)	17.6 (8.3)	23.5 (11.1)	29.1 (13.8)	34.9 (16.6)	40.3 (19.2)	45.9 (22.0)
$\langle I/\sigma(I)\rangle$	47.0 (15.3)	64.3 (23.8)	67.6 (25.0)	70.9 (27.1)	74.0 (28.7)	76.0 (29.6)	75.9 (29.6)
$R_{\rm meas}$‡ (%)	6.4 (15.8)	5.8 (13.0)	6.3 (13.1)	6.4 (12.1)	7.3 (12.7)	8.2 (13.9)	9.4 (17.3)
$R_{\rm p.i.m.}$§ (%)	1.3 (4.8)	1.0 (3.2)	0.9 (2.8)	0.8 (2.3)	0.9 (2.2)	0.9 (2.3)	1.0 (2.7)
$R_{\rm anom}$	3.8 (10.3)	3.2 (6.5)	3.1 (5.7)	3.1 (5.1)	3.0 (5.2)	3.0 (5.2)	3.0 (5.2)
Anomalous signal to noise¶	1.2 (0.7)	1.5 (0.8)	1.5 (0.8)	1.7 (0.8)	1.7 (0.8)	1.7 (0.9)	1.7 (0.8)

† Multiplicity of data for the native data set and multiplicity of the anomalous pairs for the SAD data sets. ‡ $R_{\rm meas} = \sum_{hkl}[N/(N-1)]^{1/2}\sum_i |I_i(hkl) - \langle I(hkl)\rangle|/\sum_{hkl}\sum_i I_i(hkl)$ is the multiplicity (N) independent $R_{\rm merge}$. § $R_{\rm p.i.m.} = \sum_{hkl}[1/(N-1)]^{1/2}\sum_i |I_i(hkl) - \langle I(hkl)\rangle|/\sum_{hkl}\sum_i I_i(hkl)$ is a precision-indicating R factor. ¶ $R_{\rm anom} = \sum_{hkl}|I^+ - I^-|/\sum_{hkl}(I^+ + I^-)/2$ is the ratio of the mean anomalous intensity difference to the mean reflection intensity. †† Anomalous signal to noise = $\langle \Delta F^{\pm}\rangle/\langle\sigma(F)\rangle$ is the ratio of the anomalous differences to the noise.

are often located in the first solvation shell of proteins. Dauter and coworkers described SAD phasing at the Cu $K\alpha$ wavelength of hen egg-white lysozyme using a crystal grown at a high NaCl concentration based on the anomalous signal of ten sulfurs and seven solvent Cl atoms (Dauter *et al.*, 1999).

Here, we report the *de novo* chlorine/sulfur SAD phasing of the previously unknown structure of the 14 kDa protein ATV-131, one of the major structural proteins of the archaeal virus *Acidianus* two-tailed virus (ATV), using data collected at 2.0 Å wavelength. To our surprise, one serendipitous chloride ion from the low-salt-concentration protein buffer turned out to be essential for solution of the structure. The minimal data requirements and the relative contributions of the Cl and S atoms are discussed.

2. Experimental

Details of the cloning, protein production and crystallization of ATV-131 will be given elsewhere.

2.1. Data collection

Data from ATV-131 crystals extending to 1.70 Å resolution were collected at a wavelength of 0.98 Å (12.7 keV) and 100 K on the PROXIMA 1 beamline at the SOLEIL synchrotron, Saint Aubin, France. This data set will be referred to in the following as 'native'. The space group $P6_1$ and the unit-cell parameters ($a = b = 62.5$, $c = 57.2$ Å, $\alpha = \beta = 90$, $\gamma = 120°$) are compatible with the presence of one molecule in the asymmetric unit ($V_{\rm M} = 2.28$ Å^3 Da^{-1}) and 46% solvent content.

Using the same crystal, eight consecutive data sets were collected at $\lambda = 2.0$ Å (6.20 keV) to 2.70 Å resolution (sad1–sad8, unit-cell parameters $a = b = 62.3$, $c = 57.1$ Å, $\alpha = \beta = 90$, $\gamma = 120°$). The SAD data sets were collected by rotating the crystal by 220° around the ω axis (0.5° per frame) at different angles around the κ axis (Table 1). Collecting data at a lower resolution than for the 'native' set allowed us to minimize radiation damage without compromising phasing.

2.2. Structure determination and refinement

Data were indexed, integrated and scaled using the *XDS* package (Kabsch, 1993). *XSCALE* was used on one hand for final scaling of the native data and on the other to merge and place the SAD data sets on a common scale and with the same index settings as the native data set. The *PHENIX* software suite (Adams *et al.*, 2002) was used to locate the anomalous scatterers, to calculate the initial experimental phases and for density modification and preliminary model building. Phases were extended from 2.70 to 1.70 Å and improved by solvent flattening using *DM* (Cowtan, 1994). *ARP*/*wARP* (Cohen *et al.*, 2004) was used to build the initial model, which was manually completed using *Coot* (Emsley & Cowtan, 2004) and refined with *REFMAC*5 (Murshudov *et al.*, 1997). The final model and structure factors have been deposited with the PDB (PDB code 3faj).

3. Results and discussion

3.1. Chlorine/sulfur SAD phasing of ATV-131

ATV-131 is a 14 kDa protein consisting of 131 residues, including five methionines and no cysteines. This protein has been identified as one of the major virion components of the archaeal virus *Acidianus* two-tailed virus (ATV). The ATV-131 crystal structure was solved using data sets sad1–4 (see §2), searching for four S atoms. A resolution cutoff at 3.0 Å was decided on based on the anomalous correlation being >35% and the anomalous signal/noise ratio being >1.3 at this resolution. Experimental phases were calculated using a three-site substructure and produced a good-quality electron-density map in which two helices were built by *RESOLVE* (Terwilliger, 2003; Fig. 1*a*). Phases were extended to 1.70 Å resolution using the native data and *ARP*/*wARP* automatically built 61% of the monomer in the asymmetric unit. The model was further refined against the native data. Details of the structure will be published elsewhere.

An anomalous difference Fourier map calculated with phases from the final model showed six significant peaks >5.5σ; Fig. 1*b*). Among them, the highest peak corresponds to a serendipitously bound chloride ion (Cl^-_{132}). The next two sites on the list correspond to the

Table 2
Map correlations between *MLPHARE* (MLP) or *RESOLVE* (RES) phases and phases derived from the final model refined against data sets sad1–3 to sad1–8.

Residues are considered to be 'built' by *RESOLVE* when they match the refined model.

	sad1–3			sad1–4			sad1–5			sad1–6			sad1–7			sad1–8		
	MLP	RES		MLP	RES		MLP	RES		MLP	RES		MLP	RES		MLP	RES	
Substructure	CC	CC	Built	CC	CC	Built	CC	CC	Built	CC	CC	Built	CC	CC	Built	CC	CC	Built
HySS	0.30	0.93	93	0.32	0.92	93	0.32	0.93	94	0.32	0.91	90	0.31	0.92	92	0.31	0.93	93
$Cl^-_{132}/S_{Met66}/S_{Met21}$	0.31	0.93	92	0.32	0.93	92	0.32	0.93	92	0.32	0.93	94	0.32	0.93	90	0.31	0.93	93
$S_{Met66}/S_{Met21}/S_{Met61}$	0.27	0.22	0	0.27	0.13	0	0.27	0.25	9	0.27	0.14	0	0.27	0.31	12	0.27	0.16	0
S_{Met66}/S_{Met21}	0.23	0.05	0	0.23	0.06	0	0.23	0.13	0	0.23	0.15	0	0.23	0.11	0	0.23	0.12	0
$Cl^-_{132}/Cl^-_{133}/Cl^-_{134}$	0.27	0.35	20	0.27	0.57	34	0.27	0.29	0	0.27	0.23	0	0.26	0.28	0	0.26	0.36	17
Cl^-_{132}/Cl^-_{133}	0.25	0.20	0	0.26	0.44	17	0.26	0.27	0	0.26	0.26	0	0.25	0.18	0	0.25	0.19	0
Cl^-_{132}/Cl^-_{134}	0.23	0.21	0	0.24	0.19	0	0.25	0.16	0	0.25	0.14	0	0.25	0.23	0	0.25	0.17	0
Cl^-_{133}/Cl^-_{134}	0.15	0.07	0	0.15	0.05	0	0.15	0.10	0	0.14	0.10	0	0.13	0.10	0	0.12	0.05	0
Cl^-_{132}	0.22	0.17	0	0.23	0.19	0	0.23	0.20	0	0.24	0.30	9	0.24	0.12	0	0.23	0.19	0

Met66 and Met21 S atoms. The remaining three peaks, Met61, Cl^-_{133} and Cl^-_{134}, were not found by *PHENIX AutoSol* (*HySS*). In fact, searching for six sites failed to identify new proper sites and produced a lower quality map and poorer automated building (not shown). Chloride ions rather than other putative anomalous scatterers from the solvent, such as Ca^{2+} or K^+, were assigned by chemical environment considerations and by the similarity of their peak heights compared with those of sulfur sites, which was consistent with their similar anomalous signal at $\lambda = 2.0$ Å ($f''_{Cl} = 1.1$ e$^-$ and $f''_S = 0.9$ e$^-$, in contrast to $f''_K = 1.7$ e$^-$ and $f''_{Ca} = 2.0$ e$^-$).

3.2. Relative contribution to phasing of Cl and S atoms

To test the relative contribution of the chlorine and sulfur sites to phasing, separate phasing attempts were performed. We used eight sets of heavy-atom substructures taken from the final 1.7 Å refined model: $Cl^-_{132}/S_{Met66}/S_{Met21}$ (control), $S_{Met66}/S_{Met21}/S_{Met61}$, S_{Met66}/S_{Met21}, $Cl^-_{132}/Cl^-_{133}/Cl^-_{134}$, Cl^-_{132}/Cl^-_{133}, Cl^-_{132}/Cl^-_{134}, Cl^-_{133}/Cl^-_{134} and Cl^-_{132} (Table 2). Our strategy consisted of two steps: (i) calculation of the initial phases with *MLPHARE* (Collaborative Computational Project, Number 4, 1994) at 2.7 Å resolution, refining site positions and occupancies against the anomalous differences, and (ii) improvement of phases and building of the initial model with *RESOLVE* using the *PHENIX AutoBuild* wizard. Identical program parameters were used to ensure a valid comparison of the results. Table 2 (columns sad1–4) lists for each substructure the map correlation coefficient (CC) calculated with *phenix.get_cc_mtz_mtz* between the map computed with the final phases and those calculated with the phases from either *MLPHARE* or *RESOLVE*. For the sake of comparison this procedure was also followed using the original positions found by *HySS*. As expected, the control substructure produced similar results to those obtained with the *HySS* substructure.

None of the sulfur-alone or chlorine-alone substructures were able to provide phases of sufficient quality to automatically build a complete initial model after density modification. Two substructures, namely $Cl^-_{132}/Cl^-_{133}/Cl^-_{134}$ and Cl^-_{132}/Cl^-_{133}, produced partial models on electron-density maps of poorer quality. We deduce that in this case the anomalous signal from S or Cl atoms alone is not sufficient to solve the structure. The CCs between the initial (*MLPHARE*) and the final maps calculated from the Cl^-_{132} or the S_{Met66}/S_{Met21} substructures are identical. This suggests that the main phasing power arises from the Cl^-_{132} ion. The expected ratio of the Bijvoet differences to the total protein amplitude provided by three S atoms or by three Cl^- ions at 2.0 Å wavelength is 1.15% and 1.46%, respectively (Dauter *et al.*, 2002). Compared with published S-SAD phasing data (Ramagopal *et al.*, 2003*b*), this anomalous signal should be sufficient to achieve phasing. However, the Bijvoet ratio estimation is limited by nonpredictable characteristics of the anomalous scatterers such as neighbouring atoms, occupancy and thermal motion. A closer examination of the refined atomic displacement parameters of the anomalous scatterers showed that Cl^-_{132} ($B = 16.87$ Å^2), S_{Met66} ($B = 26.03$ Å^2) and S_{Met21} ($B = 31.87$ Å^2) displayed lower values and

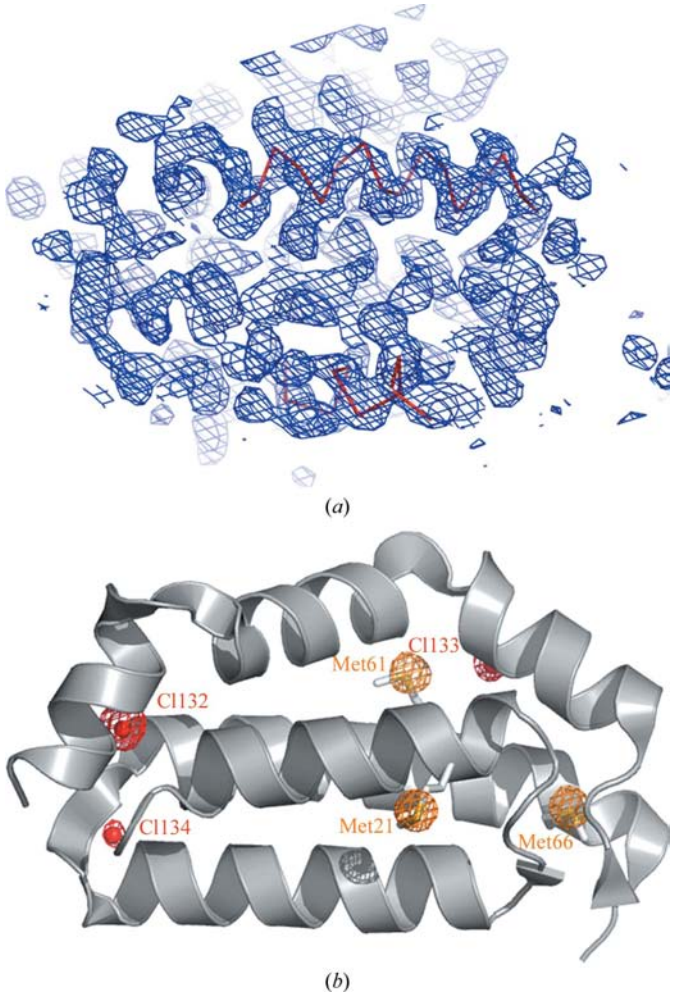

Figure 1
Experimental phasing of ATV-131. (*a*) Experimental electron-density maps and partial model obtained with *PHENIX AutoSol* using data set sad1–4. (*b*) Ribbon plot of the refined structure of ATV-131. An anomalous difference Fourier map contoured at 5.5σ shows the Cl (red) and S (orange) atoms. Images were generated with *PyMOL* (http://pymol.sourceforge.net/).

were therefore better ordered and more likely to contribute to the signal. Although Cl^-_{133} (B = 28.71 Å^2) is an exception in this respect, its chemical environment, with a single direct contact to the protein (Asn92), is clearly looser than that of Cl^-_{132}, which is tightly bound to four protein atoms from residues Thr51 and Arg110.

Therefore, we conclude that in the particular case of SAD phasing using native crystals it seems worth collecting data at a wavelength that would allow the addition of the extra anomalous signal from bound solvent atoms, as exemplified by Cl^-_{132} in the present work.

3.3. Effect of multiplicity

Despite showing reasonable indicators of anomalous signal (Table 1), the data from the low-multiplicity data set sad1–2 were not sufficient to solve the substructure using *PHENIX AutoSol* nor to produce reliable initial phases starting from the refined Cl^-_{132}/S_{Met66}/S_{Met21} substructure. Indeed, the anomalous correlation of data set sad1–2 is clearly worse than that of the sad1–4 data set used to solve the structure (Fig. 2*a*). The sad1–3 data set allowed the correct location of the Cl^-_{132}/S_{Met66}/S_{Met21} substructure and produced an 88-residue model using *RESOLVE* (Table 2).

The question arose as to whether sulfur-only or chlorine-only sites could be used to solve the ATV-131 structure provided that data with higher multiplicity were included. We performed a series of phasing tests using the same strategy as described above but with data sets of higher (from 29.1 to 45.9) anomalous multiplicity (sad1–5 to sad1–8, respectively). The final model was refined to 2.7 Å resolution against each of these merged data sets (not shown) to compare the initial (*MLPHARE*) and density-modified (*RESOLVE*) phases with their respective refined phases. In both cases *HySS* found the Cl^-_{132}/S_{Met66}/S_{Met21} substructure and *RESOLVE* returned models consisting of 90–93 residues. However, no other substructure was able to consistently produce phases of sufficient quality for complete model building using these data sets (Table 2). Only partial structures were produced for some combinations of data sets and substructures. Thus, increasing the multiplicity of the data beyond 23.5 not only did not help in phasing from the anomalous signal of Cl or S atoms solely, it also resulted in worse phasing from substructures other than Cl^-_{132}/S_{Met66}/S_{Met21}.

This result can be interpreted as a decay effect arising from radiation damage. In fact, signs of decay are evident from the values of R_{meas} and $R_{p.i.m.}$ in data sets sad6 to sad8 (Table 1). A graphical view of the continuity of decay during data collection is shown in Fig. 2(*b*), where the decay R factor (R_d) is plotted as a function of the image number (Diederichs, 2006). An anomalous multiplicity of ∼25 can thus be defined in this study as a good compromise between enhancement of the anomalous signal on one hand and restraint of the severity of radiation damage on the other.

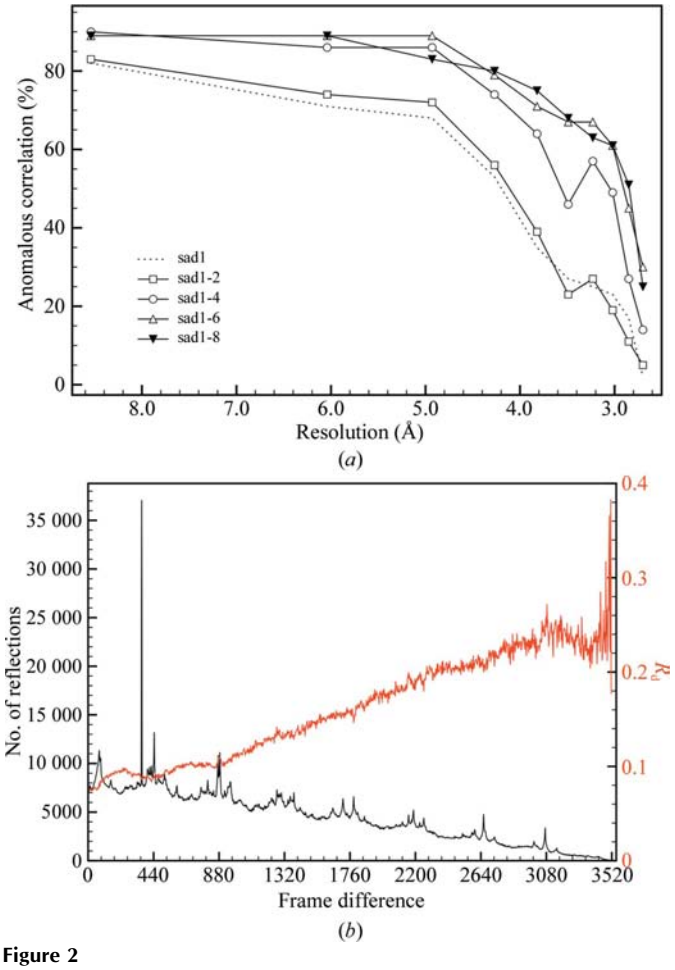

Figure 2
Anomalous signal and radiation decay. (*a*) Correlation coefficient between two separately merged parts of data sets sad1, sad1–2, sad1–4, sad1–6 and sad1–8. (*b*) The R_d indicator of decay is plotted (red) as a function of frame-number difference along with the number of reflection pairs contributing to the calculation (black). See text for details.

4. Conclusions

Selenomethonine substitution in *Escherichia coli* and heavy-atom derivatization are still time-consuming and limiting steps. On average, a protein contains 2.4 methionine and 1.7 cysteine residues per 100 amino acids (McCaldon & Argos, 1988), corresponding to an estimated Bijvoet ratio of 1.4% at 2.0 Å wavelength (assuming 7.46 non-H atoms per amino acid). To exploit this intrinsic anomalous signal and given that NaCl and KCl are part of almost every protein buffer and crystallization cocktail and that ammonium sulfate is one of the most widely used precipitants in protein crystallization, we propose the collection of accurate long-wavelength ($\lambda \simeq 2.0$ Å) SAD data from native crystals showing strong good-quality diffraction as a routine approach for *de novo* phasing. This approach would be particularly interesting for high-throughput projects, where it could avert the time-consuming preparation of heavy-atom derivatives or selenomethionine substitution.

This work was supported in part by the Marseille–Nice Génopole and by a PhD grant from the French Research Ministry to AG. We are indebted to Pierre Legrand, PROXIMA 1 beamline scientist, for his help during data collection.

References

Adams, P. D., Grosse-Kunstleve, R. W., Hung, L.-W., Ioerger, T. R., McCoy, A. J., Moriarty, N. W., Read, R. J., Sacchettini, J. C., Sauter, N. K. & Terwilliger, T. C. (2002). *Acta Cryst.* D**58**, 1948–1954.
Cohen, S. X., Morris, R. J., Fernandez, F. J., Ben Jelloul, M., Kakaris, M., Parthasarathy, V., Lamzin, V. S., Kleywegt, G. J. & Perrakis, A. (2004). *Acta Cryst.* D**60**, 2222–2229.
Collaborative Computational Project, Number 4 (1994). *Acta Cryst.* D**50**, 760–763.
Cowtan, K. (1994). *Jnt CCP4/ESF–EACBM Newsl. Protein Crystallogr.* **31**, 34–38.
Dauter, Z. & Adamiak, D. A. (2001). *Acta Cryst.* D**57**, 990–995.
Dauter, Z., Dauter, M., de La Fortelle, E., Bricogne, G. & Sheldrick, G. M. (1999). *J. Mol. Biol.* **289**, 83–92.
Dauter, Z., Dauter, M. & Dodson, E. J. (2002). *Acta Cryst.* D**58**, 494–506.

Diederichs, K. (2006). *Acta Cryst.* D**62**, 96–101.
Dodson, E. (2003). *Acta Cryst.* D**59**, 1958–1965.
Doublié, S. (1997). *Methods Enzymol.* **276**, 523–530.
Emsley, P. & Cowtan, K. (2004). *Acta Cryst.* D**60**, 2126–2132.
Garman, E. & Murray, J. W. (2003). *Acta Cryst.* D**59**, 1903–1913.
Hendrickson, W. A. & Teeter, M. M. (1981). *Nature (London)*, **290**, 107–113.
Kabsch, W. (1993). *J. Appl. Cryst.* **26**, 795–800.
McCaldon, P. & Argos, P. (1988). *Proteins*, **4**, 99–122.
Murshudov, G. N., Vagin, A. A. & Dodson, E. J. (1997). *Acta Cryst.* D**53**, 240–255.
Ramagopal, U. A., Dauter, M. & Dauter, Z. (2003*a*). *Acta Cryst.* D**59**, 868–875.
Ramagopal, U. A., Dauter, M. & Dauter, Z. (2003*b*). *Acta Cryst.* D**59**, 1020–1027.
Rice, L. M., Earnest, T. N. & Brunger, A. T. (2000). *Acta Cryst.* D**56**, 1413–1420.
Salgado, P. S., Walsh, M. A., Laurila, M. R. L., Stuart, D. I. & Grimes, J. M. (2005). *Acta Cryst.* D**61**, 108–111.
Terwilliger, T. C. (2003). *Acta Cryst.* D**59**, 38–44.
Wang, B.-C. (1985). *Methods Enzymol.* **115**, 90–112.
Zwart, P. H. (2005). *Acta Cryst.* D**61**, 1437–1448.